Online Appendix

This online appendix supports the paper "Pricing Uncertainty Induced by Climate Change" by Michael Barnett, William Brock and Lars Peter Hansen. We give a special acknowledgment to Jieyao Wang for her lead role in computations.

A Model Specification

In the body of the paper, we specified the model with adjustment costs in the investment equation. Alternatively, we could posit the adjustment costs in the output constraint. This model is sufficiently streamlined so that the solution allows for both interpretations.[1] The choice of interpretation affects how we relate this model to actual investment data when calibrating the model.

For the modified adjustment cost formulation, define an alternative investment/capital ratio equal to

$$\frac{\widetilde{I}_t}{K_t} = \phi_0 \log\left(1 + \phi_1 \frac{I_t}{K_t}\right).$$

Substituting into the capital evolution give us

$$dK_t = K_t \zeta_K(Z_t)dt + \widetilde{I}_t dt + K_t \sigma_K \cdot dW_t.$$

Inverting this relationship we have that

$$\frac{I_t}{K_t} = \frac{\exp\left(\frac{\widetilde{I}_t}{\phi_0 K_t}\right) - 1}{\phi_1}.$$

Now the output equation can be written with convex adjustment costs as

$$C_t + K_t \left[\frac{\exp\left(\frac{\widetilde{I}_t}{\phi_0 K_t}\right) - 1}{\phi_1}\right] + J_t = \alpha K_t.$$

This change impacts how to construct a measurement counterpart for investment in this model.

[1] This argument was pointed out to us by Paymon Khorrami and Fabrice Tourre.

B Social Cost of Carbon

As in the body of the paper, consider impulse response functions for the logarithm of damages in the future induced by a marginal change in emissions today. The responses are necessarily nonlinear impulse responses and hence will be state-dependent. The marginal emissions change induces an impact on $\log D_{t+u}$ given by[2]

$$\left([\nabla\Gamma](\beta F_t)\beta + \zeta_D(Z_t)\cdot\begin{bmatrix}1\\0\end{bmatrix}\right) + \int_0^u [\nabla^2\Gamma](\beta F_{t+\tau})\beta^2 E_{t+\tau}d\tau.$$

The first contribution occurs on impact, and the second one accumulates through the effect of current emissions on the state variable f.

Consider the specification where damages enter the utility function discounted and multiplied by $\delta(1-\kappa)$. Recall that by doing some simple accounting and exploiting the exponential discounting used for the discounted marginal damage response, we ecombine all the date τ contributions for $u \geqslant \tau$ to obtain

$$\exp(-\delta\tau)(1-\kappa)[\nabla^2\Gamma](\beta F_{t+\tau})\beta^2 E_{t+\tau},$$

along with the initial term

$$\exp(-\delta\tau)\delta(1-\kappa)\left([\nabla\Gamma](\beta F_t)\beta + \zeta_D(Z_t)\cdot\begin{bmatrix}1\\0\end{bmatrix}\right).$$

The external part to the social cost of carbon is the expected exponentially discounted future impulse responses. In the absence of ambiguity and robustness concerns it is given by

$$\begin{aligned}&\delta(1-\kappa)\left([\nabla\Gamma](\beta F_t)\beta + \zeta_D(Z_t)\cdot\begin{bmatrix}1\\0\end{bmatrix}\right)\int_0^\infty \exp(-\delta\tau)d\tau\\ &+ E\left[\int_0^\infty \exp(-\delta\tau)(1-\kappa)[\nabla^2\Gamma](\beta F_{t+\tau})\beta^2 E_{t+\tau}d\tau \mid X_t = x\right]\end{aligned} \tag{B.1}$$

divided by the date t marginal utility of consumption.

By integrating the exponential function in the first expression, the δ drops out resulting

[2]Following our earlier notational convention, $[\nabla^2\Gamma]$ denotes the second derivative of Γ.

in

$$(1-\kappa)\left([\nabla\Gamma](\beta F_t)\beta+\zeta_D(Z_t)\cdot\begin{bmatrix}1\\0\end{bmatrix}\right),$$

which is one of the two terms in formula (B.1) for *ecc.*

Since the second term is a discounted expected value, it solves a so-called "Feynman-Kac (FK) equation." Formally, we are interested in the solution Φ to the forward-looking equation

$$\begin{aligned}\Phi(X_t)&=\mathbb{E}\left[\int_0^\infty \exp(-\delta\tau)\Psi(X_{t+\tau})d\tau \mid X_t\right]\\&=\exp(\delta t)\int_t^\infty \exp(-\delta\tau)\mathbb{E}\left[\Psi(X_\tau)\mid X_t\right]d\tau\end{aligned}\tag{B.2}$$

for a pre-specified Ψ. Specifically, let

$$\Psi(x)=(1-\kappa)[\nabla^2\Gamma](\beta f)\beta^2 e^*(x)\exp(r).$$

To provide a heuristic reminder of form and rationale for the FK equation, we obtain the drift of the process $\{\Phi(X_t):t\geqslant 0\}$ of the left-hand hand side of (B.2) via Ito's formula for $X_t=x$ as

$$\frac{\partial\Phi}{\partial x}(x)\cdot\mu_X[x,a^*(x)]+\frac{1}{2}\text{trace}\left[\sigma_X(x)'\frac{\partial^2\Phi}{\partial x\partial x'}(x)\sigma_X(x)\right],$$

where a^* is the maximizing decision rule. Differentiating the right-hand side of (B.2) with respect to t gives an alternative formula for this drift:

$$\delta\Phi(x)-\Psi(x).$$

By equating these, we obtain the FK or (more generally) resolvent equation:

$$-\delta\Phi(x)+\frac{\partial\Phi}{\partial x}(x)\cdot\mu_X[x,a^*(x)]+\frac{1}{2}\text{trace}\left[\sigma_X(x)'\frac{\partial^2\Phi}{\partial x\partial x'}(x)\sigma_X(x)\right]+\Psi(x)=0.\tag{B.3}$$

By differentiating the HJB equation with respect to f and applying the "Envelope Theorem," it can be shown that the solution Φ to the FK equation satisfies

$$\Phi(x)=-V_f(x).$$

The analogous arguments apply in the presence of ambiguity and robustness concerns except that we use the altered probability distribution when computing expectations.

C Numerical Method

To solve the nonlinear partial differential equations that characterize the HJB equations for the planner's problems from our model, we use a so-called implicit, finite-difference scheme and a conjugate gradient method.[3] We briefly outline the steps to this numerical solution method below.

Recall that the HJB equation of interest for the consumption damages model includes both minimization and maximization:

$$\begin{aligned} 0 = \max_{a\in\mathbb{A}} \min_{q>0,\int qP(d\theta)=1} \min_{g\in\mathbb{R}^m} & -\delta V(x) + \delta(1-\kappa)\left[\log\left(\alpha - i - j\right) + k - d\right] + \delta\kappa\left(\log e + r\right) \\ & + \frac{\partial V}{\partial x}(x)\cdot\left[\int_\Theta \mu_X(x,a\mid\theta)q(\theta)P(d\theta) + \sigma_X(x)g\right] \\ & + \frac{1}{2}\text{trace}\left[\sigma_X(x)'\frac{\partial^2 V}{\partial x\partial x'}(x)\sigma_X(x)\right] \\ & + \frac{\xi_m}{2}g'g + \xi_p\int_\Theta[\log q(\theta)]q(\theta)P(d\theta). \end{aligned}$$

We proceed recursively as follows:

i) start with a value function guess $\widetilde{V}(x)$ and a decision function $\widetilde{a}(x)$;

ii) given $(\widetilde{V},\widetilde{a})$, solve the minimization problem embedded in the HJB equation and produce an exponentially-tilted density $\widehat{q}$ and drift distortion $\widehat{g}$ conditioned on x and using the approach described in Section D;

iii) compute the implied relative entropy from the change in prior:

$$\widehat{\mathbb{I}}(x) = \int_\Theta[\log\widehat{q}(\theta)]\widehat{q}(\theta)P(d\theta);$$

[3]Consultations with Joseph Huang, Paymon Khorrami and Fabrice Tourre played an important role in the software implementation.

iv) solve the following maximization problem by choice of $a = (i, j, e)$:

$$\begin{aligned}&\delta(1-\kappa)\log(\alpha - i - j) + \delta\kappa\log e \\ &+ \frac{\partial V}{\partial x}(x)\cdot\int_\Theta \mu_X(x, a \mid \theta)\,\widehat{q}(\theta \mid x)P(d\theta);\end{aligned}$$

a) Compute $\hat{i}$ and $\hat{j}$ by solving the two first-order conditions for i and j with cobweb-style iterations. Cobweb iterations converge or diverge depending the relative slopes of supply and demand functions. By shrinking the step size, these slopes can be altered. Expand the two equation system by adding a third equation that defines a common "price" p,

$$p = \frac{\delta(1-\kappa)}{\alpha - i - j} = g(i+j).$$

Write the two first-order conditions as

$$p = \frac{\phi_0\phi_1 V_k(x)}{1+\phi_1 i} = f_1(i)$$

$$p = V_r(x)\,(\psi_0\psi_1)\,j^{\psi_1 - 1}\exp\left[\psi_1(k-r)\right] = f_2(j).$$

Given p and for step size $\tilde{\epsilon}$, compute

- $i^* = (f_1)^{-1}(p)$
- $j^* = (f_2)^{-1}(p)$
- $p^* = \tilde{\epsilon}g(i^* + j^*) + (1-\tilde{\epsilon})\,p$
- set $p = p^*$.

Iterate to convergence.

b) Compute $\hat{e}$ by solving the first-order conditions

$$\frac{\delta\kappa}{e} + \frac{d}{de}\left[V_x(x)\cdot\int_\Theta \mu_X(x, i, j, a \mid \theta)\,\widehat{q}(\theta \mid x)P(d\theta)\right] = 0.$$

These first-order conditions turn out not to depend on (i, j).

v) use the minimization output from step (ii) and maximization output from step (iv) and construct an adjusted drift using the following formula, which is the analog to formula (20):

$$\widehat{\mu}(x) = \int_\Theta \mu_X(x, \widehat{a} \mid \theta)\,\widehat{q}(\theta \mid x)P(d\theta) + \sigma_X(x)\widehat{g}(x);$$

vi) construct the linear equation system for a new value function $V = \widehat{V}$:

$$\begin{aligned} 0 = &- \delta V(x) + \delta(1-\kappa)\left(\log\left[\alpha - \widehat{i}(x) - \widehat{j}(x)\right] + k - d\right) + \delta\kappa\left[\log\widehat{e}(x) + r\right] \\ &+ \frac{\partial V}{\partial x}(x)\cdot\widehat{\mu}(x) + \frac{1}{2}\text{trace}\left[\sigma_X(x)'\frac{\partial^2 V}{\partial x \partial x'}(x)\sigma_X(x)\right] \\ &+ \frac{\xi_m}{2}\widehat{g}(x)\cdot\widehat{g}(x) + \xi_p\widehat{\mathbb{I}}(x); \end{aligned}$$

vii) modify this equation by adding a so-called "false transient" to the left-hand side:

$$\begin{aligned} \frac{V(x) - \widetilde{V}(x)}{\epsilon} = &- \delta V(x) + \delta(1-\kappa)\left(\log\left[\alpha - \widehat{i}(x) - \widehat{j}(x)\right] + k - d\right) + \delta\kappa\left[\log\widehat{e}(x) + r\right] \\ &+ \frac{\partial V}{\partial x}(x)\cdot\widehat{\mu}(x) + \frac{1}{2}\text{trace}\left[\sigma_X(x)'\frac{\partial^2 V}{\partial x \partial x'}(x)\sigma_X(x)\right] \\ &+ \frac{\xi_m}{2}\widehat{g}(x)\cdot\widehat{g}(x) + \xi_p\widehat{\mathbb{I}}(x); \end{aligned} \tag{C.1}$$

viii) solve linear system (C.1) for $V = \widehat{V}$ using a conjugate-gradient method;

ix) set $\widetilde{V} = \widehat{V}$ and $\widetilde{a} = \widehat{a}$ and repeat steps (ii) - (viii) until convergence.

Remark C.1. *We discretize the state space of x using a set number of points along each of the three dimensions and impose a fixed step size between points for each of these dimensions. For interior points, we approximate the first derivatives using a first-order upwind scheme while the second derivatives are calculated using a central difference scheme. Upwind schemes are one-sided difference approximations that use the sign of the drifts for the states to determine the direction of the difference. (See, for instance, "An Introduction to Finite Difference Methods for PDE methods in Finance" by Agnes Tourin, Fields Institute.) At boundary points we sometimes only have one option used in the approximation. We use a symmetric second difference approximation whenever possible and switch to a one-sided approximation as needed at boundary points. With this construction, we have reduced the right-hand side of equaton in step vii) as a matrix applied to the value function at the chosen set of discrete points.*

Remark C.2. *We solve the matrix counterpart to the equaion in step (viii) using the conjugate gradient algorithm. This is a well known iterative algorithm designed to solve*

a minimization problem: $\frac{1}{2}(\Lambda y - \lambda)'(\Lambda y - \lambda)$ *for a nonsingular matrix* Λ *and vector* λ*. The* y *that minimizes this expression satisfies the linear equation* $\Lambda y = \lambda$*. The matrix* Λ *and vector* λ *come from the numerical approximation of equation (22). We measure the conjugate gradient error by*

$$\sqrt{\frac{(\Lambda y - \lambda)'(\Lambda y - \lambda)}{\lambda'\lambda}}. \tag{C.2}$$

We prespecify a conjugate gradient error bound and a bound on the difference in value functions between iterations and take as the starting point for conjugate gradient the output from the previous iteration. We achieve convergence when the difference in value functions between iterations satisfies a prespecified error bound. Upon convergence, we compute the maximum error for the matrix approximation to the right-hand side of equation system in step C.1. We call this the maximum pde error.

Remark C.3. *The choices of* $\tilde{\epsilon}$ *in step (iv) and* ϵ *in step (vii) are made by trading off increases in speed of convergence, achieved by increasing their magnitudes, and enhancing stability of the iterative algorithm, achieved by decreasing their magnitudes.*

Remark C.4. *While we are computing one-sided difference approximations at boundary points, we are not imposing additional boundary conditions on our finite state space as is often done when solving pde's with regular boundaries. Instead we aim to approximate pde solutions for the stochastic differential equation with unattainable boundaries.*

We solved the specification with damages to the growth rate with the same steps applied to the corresponding HJB equation. Other than altering how damages enter the model, the key difference for the growth-rate setting is the computation of the minimizing probabilities, which we discuss in the next section.

D Computing Ambiguity-Adjusted Probabilities

In our implementations, we presume a discrete number of possible damage function specifications along with a normal distribution for the climate sensitivity β.

We consider two particular cases, the first is pertinent when climate damages alter the growth rate of capital and the second when damages proportionately reduce consumption.

i) Each possible Γ is a quadratic function. In this case, we proceed as follows: we deduce the implied q by first determining the probability distribution for β conditioning on the

Γ specification. It is straightforward to show that these conditional distributions are normal with altered means and variances. We also have a quasi-analytic formula for the implied relative entropy conditioned on the Γ specification since both the baseline and altered distributions for β are normal. We then deduce the implied discrete weights on the alternative Γ specifications and produce the full measure of entropy inclusive of these discrete components.

ii) One of the Γ's is not a quadratic function. This is true for the high damage specification acting through the preferences. In this case, we must do numerical integration to compute the implied q's, the relative entropies, and the resulting ambiguity adjusted drift coefficient. We use Gaussian-Legendre quadrature in our computations.

For the growth specification, we construct nine models for Γ as follows. We take the approximating normal distribution from Burke et al. (2018) for their linear and quadratic coefficient estimates. In effect, this treats their asymptotic approximation as a prior for our analysis. We take a Cholesky decomposition of the covariance matrix and the corresponding linear transformation of the coefficients so as to obtain a bi-variate standard normal distribution. With a three point Gaussian-Hermite quadrature for each dimension, we generate nine implied models for Γ with the Gaussian-Hermite weights scaled to sum to one as the baseline probabilities. Had the SCC not been so substantial, we would have been more concerned about "lopping off tails" with so few points of approximation.

E Backing Out Parameters

Our approach to calibration is to invert the previous equations taking the steady states for (i, e, y, π) and the growth rate η as inputs for determining (ν, c, j) along with the production parameters. There is a nice recursive structure, which we exploit in the following steps.

i) Compute (c, ν) from the first-order conditions for e and the formula for π:

$$\frac{\delta\kappa}{e} = \nu = 1 - \left[\frac{\delta(1-\kappa)}{c}\right]\pi$$

ii) Given (i, π) and η, we solve for the capital evolution parameters.

a) From the first-order conditions for investment, solve

$$\pi = 1 + \phi_1 i$$

for ϕ_1, where we have set $\phi_0\phi_1 = 1$.

b) From the growth equation,

$$\eta = \overline{\mu}_K + \phi_0 \log(1 + \phi_1 i),$$

solve for $\overline{\mu}_K$ given η, ϕ_0, and ϕ_1.

iii) Given (η, c, y, e), we have three equations for the three unknowns (ψ_0, ψ_1) and $\log j$ based on the first-order conditions for j, the state equation for reserves, and the co-state equation for reserves:

$$\log\left[\frac{\delta(1-\kappa)}{c}\right] = \log\nu + \log\psi_0 + \log\psi_1 + (\psi_1 - 1)\log j - \psi_1 y,$$
$$\log(\eta + e) = \log\psi_0 + \psi_1 \log j - \psi_1 y,$$
$$\log(e - \delta) = \log\psi_0 + \log\psi_1 + \psi_1 \log j - \psi_1 y.$$

It is most convenient to transform this equation system.

a) By subtracting the first and third equations, we get

$$\log\left[\frac{\delta(1-\kappa)}{c}\right] - \log(e - \delta) = \log\nu - \log j,$$

which we use to solve for $\log j$.

b) Substituting $\log j$ into the second equation gives a linear equation for ψ_1 expressed in terms of $\log\psi_0$.

c) Substituting this expression for ψ_1 into the third equation gives us a single equation to solve in a single unknown, $\log\psi_0$.

iv) Given (c, i, j) determine α from the output constraint by adding them together. It may be verified that $\alpha = i + \delta\pi$.

These equations may not be solvable for some empirical inputs, but they do have solutions for the inputs that we used.

F Some Empirical Evidence

Our model is highly stylized, making it challenging to find precise inputs to use as calibration targets. To implement the approach in Section E, we set the growth rate η at 2%, and the reserve capital ratio at .98. We will return to this second number later when we discuss initial conditions. Our number for the emissions-to-reserves ratio is .015. While this ratio is less than that used by Bornstein et al. (2017), theirs is only based on oil. (Their ratio is between .026 to .028.) We use a smaller number to incorporate coal, based in part on numbers from BP (2018) and Figueres et al. (2018).[4]

There are four preference parameters that are pertinent $(\delta, \kappa, \xi_p, \xi_m)$ to our analysis. In our reported computations, we abstracted from model misspecification concerns and effectively set $\xi_m = \infty$. In the Section 4.1, we discussed discounting in valuation for which the subjective discount rate, δ, is only part of the story. Stochastic growth and uncertainty aversion, which we feature, are important contributors. In Section 5, we argued that the implied worst-case probabilities or their relative entropies are easier to interpret than the numerical value of ξ_p. The actual numerical values for ξ_p are $\frac{1}{4000}$ for the proportional damages in preferences specification and $\frac{1}{175}$ for the damages to growth rates specification. Finn (1995) and Leduc and Sill (2004) use .04 as the value of the energy input share which we deflate by 80% based on the approximate proportion of energy consumption that comes from fossil fuels. For instance, see data from the International Energy Agency (IEA) Statistics database. Thus, we use $\kappa = .032$ in our computations.

Consider next the technology parameters for capital accumulation and productivity. For such a stylized model, there is no agreed upon way to fit parameters to measured counterparts of steady states. We agree with Pindyck and Wang (2013) that capital within this model should be interpreted broadly to include both human, intangible, as well as organizational capital. Even for more narrow views of capital, there is a rather substantial range for the magnitude of the adjustment costs. We set the steady state $\pi = 2.5$ and the investment-capital ratio to be .09. Although not critical to computation, the implied investment-capital ratio is sensitive to whether the costs are presumed on the input or output side of the capital evolution. This number would be the substantially lower (.055) had we used the alternative construction given in Appendix A.

The capital and oil reserves volatility σ_K, σ_R are vectors where the relevant entries are

[4]Specifically, we choose an initial period emissions target of about 10 GtC/yr in our calibrations to match the most recent number from Figueres et al. (2018).

chosen to match the empirically measured annual percent changes in the time series of GDP and reserves from the World Bank database and BP (2018). We assume $\sigma_K \cdot \sigma_R = 0$, and so $\sigma_K = [.0161, 0, 0]'$ and $\sigma_R = [0, .0339, 0]'$. Given the structure of our model and focus on smooth ambiguity in the computational analysis, σ_d is inconsequential for the calculations that we report.

Table F.1: Initial Values

Y_0	80
K_0^a	695.65
R_0	650
F_0	290

[a] K_0 is derived from $K_0 = Y_0/\alpha$

The initial values for the model solution simulations are given in Table F.1. The value for GDP comes from the World Bank database and the capital value is implied by the assumed productivity parameter α and this GDP value. The value for reserves comes from estimates of existing recoverable reserves of oil and coal from the U.S. Energy Information Administration (EIA), BP (2018), empirical measures of reserves cited by McGlade and Ekins (2015) (who provide detailed information on the reserves data, including the EIA and BP estimates), and earlier research by Rogner (1997). By construction, the ratio of the initial reserves to capital matches the steady state value used in setting the steady state target y. The initial value of cumulative emissions or atmospheric carbon concentration comes from the NOAA dataset. We use anomaly from the preindustrial level, where the preindustrial level we use is 580, in line with the IPCC Fourth Assessment Report (2007) for concentrations around 1800. The Carbon Dioxide Information Analysis Center (CDIAC) provides a conversion factor to convert the NOAA and IPCC concentrations values from parts per million (ppm) to gigatons of carbon (GtC).

G More Computations

In this section we consider some calculations associated with alternative model configurations which we use to supplement the findings reported in the text.

G.1 Abstracting from the climate externality

While we reported previously the social cost of carbon for the socially efficient allocation, we now show the difference when we produce analogous computations under the competitive allocation. While these are not directly transformable into Pigouvian taxes, they do reveal the implied social costs for marginal changes in emissions. Under the competitive allocation the costs are substantially higher because the allocations are much more damaging to the economy. This is evident in Figure G.1 which shows much higher cost trajectories when the market economy ignores climate damages. We limit the time horizon for Figure G.1 to 60 years because the difference in the SCC is so drastic for longer horizons.

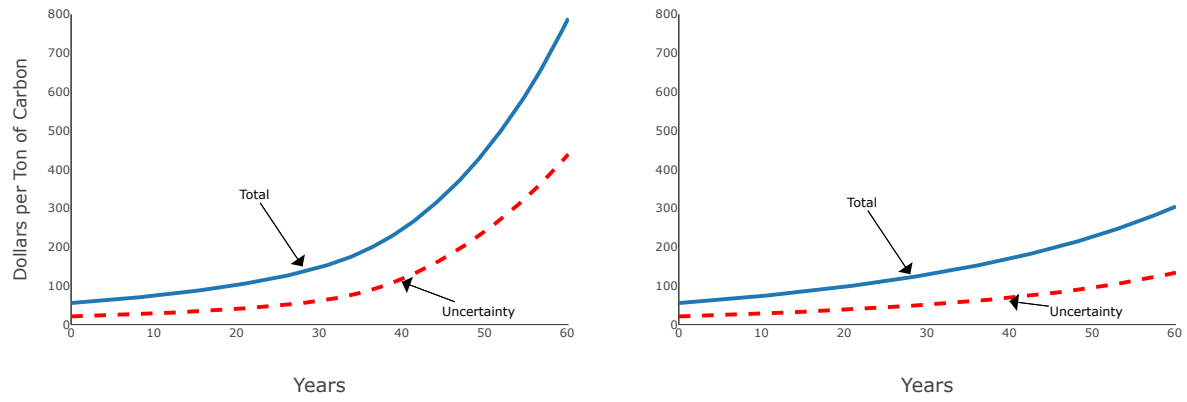

Figure G.1: Social cost of carbon comparison for alternative allocations. The left panel imposes the competitive allocation ignoring the climate externality. The right panel imposes the social planner's solution and reproduces Figure 6. The right panel plots use a shorter time period than in Figure 6 to facilitate comparisons to the computations with the competitive allocaiton. The blue solid curve represents the total SCC, and the red dashed curve represents the uncertainty contribution.

Figure G.2 compares the two emissions trajectories. Since the competitive solution ignores the climate externality, it increases along a balanced growth path. In contrast, the trajectory from the social planner's problem decays because of the potential for serious damages to the environment.

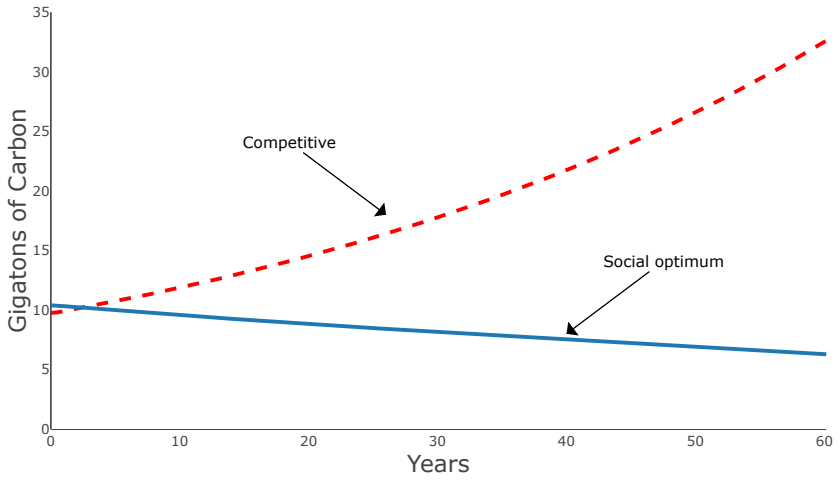

Figure G.2: Emissions comparison for alternative allocations. The blue solid curve reproduces the emissions trajectory for the social planner and is reproduced from from Figure 7 in the paper. The red dashed curve shows the emissions trajectory for the competitive allocation.

Table G.1 compares the relative entropies under the competitive allocation with those for the planner's problem. In addition, the implied worst-case probabilities for the low damage specification are provided in parentheses. Given that ξ_p is held fixed, the relative entropies of the implied worst-case probabilities are larger under the competitive allocation.

	Competitive allocation	Planner's allocation
Year	Entropies (prob)	Entropies (prob)
0	.005 (.50)	.005 (.50)
30	.019 (.50)	.011 (.50)
60	.343 (.32)	.053 (.49)

Table G.1: Relative entropies and implied worst-case probabilities for the consumption damage specification. The left-panel evaluations are under the competitive allocation, and the right-panel evaluations are under the allocation under the planner's solution.

G.2 Omitting investment in exploration

Next we explore the impact of exploration. We display the SCC comparisons in Figure G.3 starting from the same initial conditions. As we see from the left panel of this figure,

the SCC is substantially higher without the possibility of exploration. This is driven by a significantly higher private contribution to the SCC, which now dominates, whereas the uncertainty adjustment is inconsequential. Without the opportunity to invest in exploration, this is a Hotelling-type model and the finite stock constraint imposed by reserves dominates the damage contribution. This is in sharp contrast to what happens when we allow for exploration.

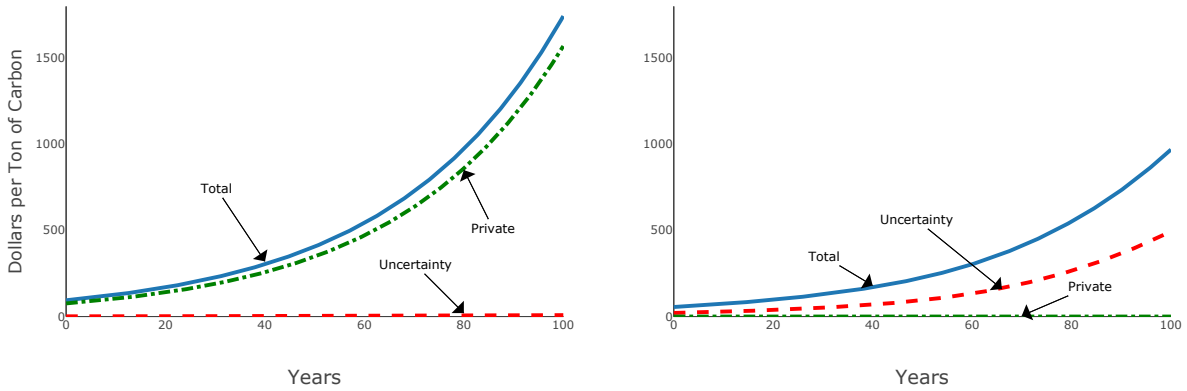

Figure G.3: Social cost of carbon across different reserve settings. The left panel precludes investment in exploration while the right panel allows for this investment. The right panel replicates Figure 6 in the paper. The blue solid curves represent the total SCC, and the red dashed curves represent the uncertainty contribution. The green dot-dashed curves represent the private contributions that do not account for damages to the climate.

The emissions trajectories for the two economies are reported in Figure G.4. Not surprisingly, emissions are lower when we preclude exploration.

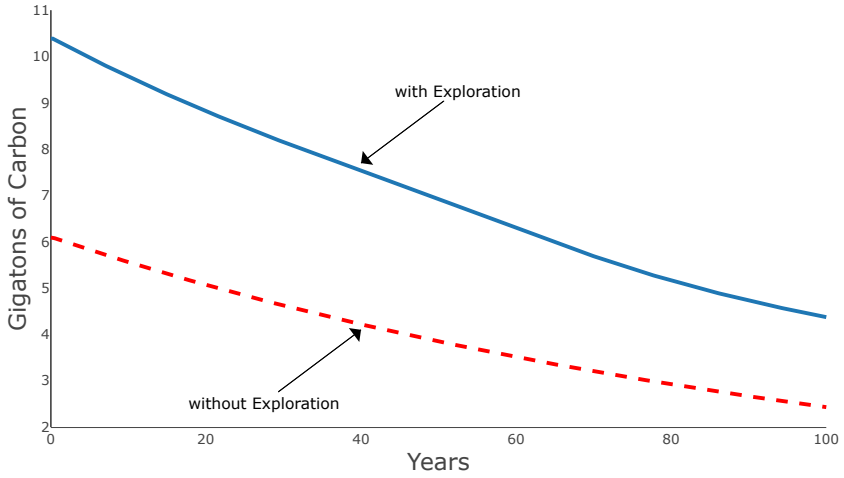

Figure G.4: Emissions comparison. The blue solid curve reproduces the emissions trajectory from Figure 7 in the paper while the red dashed curve shows results for our economy without investment in exploration.

Table G.2 reports the relative entropies and worst-case probabilities for the specifications with two different initializations for the stock reserves. Exploration is closed down for these runs. Consistent with the small uncertainty contribution to the SCC in the absence of exploration and the reserve stock initialized at 650, we find that the relative entropies are very small and probability adjustments for the damage configurations are negligible in this case. Increasing the stock of reserves to 9000 changes substantially this finding.

Year	Reserves = 650	Reserves = 9000
	Entropies (prob)	Entropies (prob)
0	.002 (.50)	.005 (.50)
25	.002 (.50)	.010 (.50)
50	.002 (.50)	.026 (.49)
75	.002 (.50)	.112 (.46)
100	.002 (.50)	.197 (.42)

Table G.2: Relative entropies for different initial reserves without exploration

Once we exclude exploration, arguably we should increase substantially the stock of reserves in the calibration to include "potential reserves." When we initialize the stock at 9000, we obtain essentially the same emissions and SCC trajectories as we found with

exploration. This larger reserve stock effectively makes the Hotelling constraint irrelevant when damages are present. See McGlade and Ekins (2015) for some rough estimates of the stock of potential reserves, which we use as motivation to introduce such a substantially larger initialization.

G.3 Using damaged consumption as the numeraire

As we noted in Section 4 of the paper, it is of potential interest to use damaged consumption as the numeraire for the SCC computations. For the time horizons that we report results, we verified that this change has negligible implications. In contrast, for longer simulations actual damages become more pronounced and the implications for the SCC become much more pronounced.

G.4 Ambiguity in the damage evolution

When climate damages alter the macroeconomic growth rate, parameter ambiguity spills over to the evolution of the SCC. In Table G.3 we report the SCC and the corresponding relative entropies under two different simulation protocols for damages, one in which we replace unknown parameters by their means and the other under the associated worst-case evolution. Interestingly, the SCC numbers are lower under the worst-case simulation because of the more sluggish capital evolution.

Year	Base-case		Worst-case	
	SCC total	SCC uncertainty	SCC total	SCC uncertainty
0	411	209	411	209
50	1,168	590	1,079	545
100	3,244	1,638	2,745	1,386

Table G.3: SCC when climate damages alter macroeconomic growth under two trajectories. The base-case simulation sets shocks to zero and uses parameter averages for damage evolution. The worst-case simulation also sets the shocks to zero but uses the worst-case distributions for averaging the unknown parameters period by period.

Importantly, the dynamic implications, including the relative importance of uncertainty, that we featured in the body of our paper remain regardless of which simulation setting we use for the analysis.

H Impulse Response Approximation to Climate Dynamics

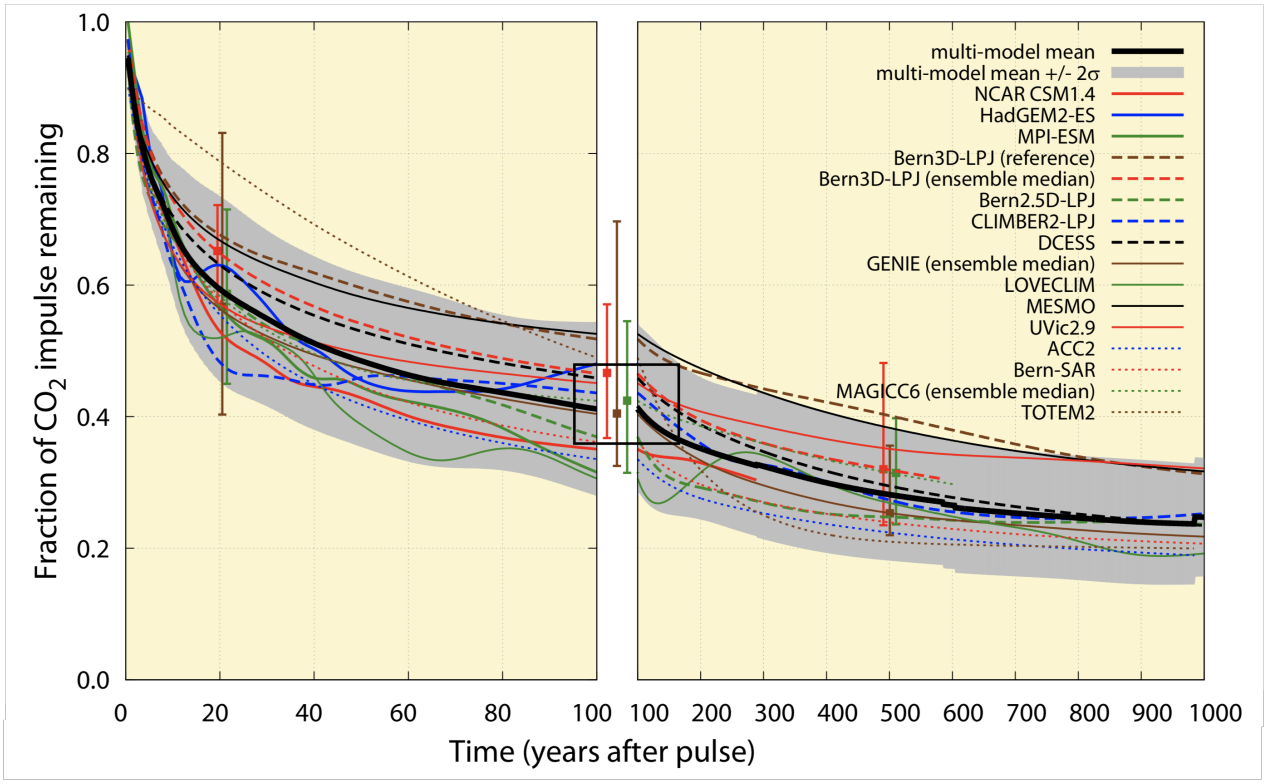

Figure H.1: This figure shows the cross model heterogeneity in carbon-climate responses. It reproduces Figure 1A of Joos et al. (2013).

In this section we report findings using the impulse response approximations from Joos et al. (2013) that illustrate cross-model heterogeneity and speak to the potential importance of model ambiguity in decision making. Figure H.1 shows the responses for long-term changes in carbon concentration. In looking at the left panel, all models agree that the impact of a change in emissions decays, but not to zero, and that the decay is very slow. After 100 years, alternative models have substantial differences in terms of their implications for carbon concentration. The impact of emissions continues to decline over future centuries, but this additional decay is remarkably slow. While there are considerable similarities in the pattern of the responses, there is substantial variation in the magnitudes

of the responses.[5] The corresponding temperature responses display more erratic behavior as reported in Joos et al. (2013) for the reasons they describe. Castruccio et al. (2014) provide further evidence for cross model differences in temperature responses to changes in radiative forcing.

We present this evidence to suggest further important research to be done that incorporates model uncertainty from climate science and to suggest some of the challenges that embracing this evidence entails.

[5]We invite the reader to inspect other figures in Joos et al. (2013) that illustrate model heterogeneity of responses of surface temperature, ocean temperature, sea level rise and other variables of interest to emission pulses of CO_2.

References

Bornstein, Gideon, Per Krusell, and Sergio Rebelo. 2017. Lags, Costs, and Shocks: An Equilibrium Model of the Oil Industry. NBER Working Paper 23423, National Bureau of Economic Research, Inc.

BP. 2018. *Statistical Review of World Energy*, vol. 67. BP.

Burke, Marshall, W. Matthew Davis, and Noah S. Diffenbaugh. 2018. Large Potential Reduction in Economic Damages Under UN Mitigation Targets. *Nature* 557:549–553.

Castruccio, Stefano, David J McInerney, Michael L Stein, Feifei Liu Crouch, Robert L Jacob, and Elisabeth J Moyer. 2014. Statistical Emulation of Climate Model Projections Based on Precomputed GCM Runs. *Journal of Climate* 27 (5):1829–1844.

Figueres, Christiana, Corinne Le Quéré, Anand Mahindra, Oliver Bäte, Gail Whiteman, Glen Peters, and Dabo Guan. 2018. Emissions Are Still Rising: Ramp Up the Cuts. *Nature* 564:27–30.

Finn, Mary G. 1995. Variance Properties of Solow's Productivity Residual and Their Cyclical Implications. *Journal of Economic Dynamics and Control* 19 (5-7):1249–1281.

Joos, F., R. Roth, J. S. Fuglestvedt, G. P. Peters, I. G. Enting, W. Von Bloh, V. Brovkin, E. J. Burke, M. Eby, N. R. Edwards, T. Friedrich, T. L. Frölicher, P. R. Halloran, P. B. Holden, C. Jones, T. Kleinen, F. T. Mackenzie, K. Matsumoto, M. Meinshausen, G. K. Plattner, A. Reisinger, J. Segschneider, G. Shaffer, M. Steinacher, K. Strassmann, K. Tanaka, A. Timmermann, and A. J. Weaver. 2013. Carbon Dioxide and Climate Impulse Response Functions for the Computation of Greenhouse Gas Metrics: A Multi-Model Analysis. *Atmospheric Chemistry and Physics* 13 (5):2793–2825.

Leduc, Sylvain and Keith Sill. 2004. A Quantitative Analysis of Oil-Price Shocks, Systematic Monetary Policy, and Economic Downturns. *Journal of Monetary Economics* 51 (4):781–808.

McGlade, Christophe and Paul Ekins. 2015. The Geographical Distribution of Fossil Fuels Unused When Limiting Global Warming to 2 °C. *Nature* 517 (7533):187–190.

Pindyck, Robert S. and Neng Wang. 2013. The economic and policy consequences of catastrophes. *American Economic Journal: Economic Policy* 5 (4):306–399.

Rogner, H-H. 1997. An Assesment of World Hydrocarbon Resources. *Annual Review of Energy and the Environment* 22:217–262.